Low Molecular Weight Fluorescent Probes for the Detection of Organophosphates

Rashid Mia[a], Peter J. Cragg[b], and Karl J. Wallace[a]*

a) Department of Chemistry and Biochemistry, University of Southern Mississippi, Hattiesburg, MS 39406 USA.

b) School of Pharmacy and Biomolecular Sciences, University of Brighton, Brighton, BN2 4GJ, UK.

Abstract

Three Low Molecular Weight Fluorescent probes (LMFPs) coumarin-enamine (**3a-c**) have been synthesized, and their photophysical properties have been studied in different solvent systems (DMSO, CH_3CN, DMF, MeOH, EtOH, Me_2CO, $MeCO_2Et$, $CHCl_3$, C_6H_5Me, and C_6H_6). Dimethyl sulfoxide was chosen as the optimum solvent to investigate **3a** for organophosphate detection. On deprotonation of the oxime, a significant spectroscopic shift is observed in the UV-Vis spectrum ($\Delta \approx 35$ nm). The fluorescence spectrum shows a broad featureless band at 535 nm that shifts hypochromically. Both the UV-vis and fluorescence spectra undergo drastic optical responses when the OP-adduct is formed. Diisopropyl chlorophosphate was found to have the most extensive changes among the phosphorus (V) center OPs investigated (diisopropyl chlorophosphate, diisopropyl fluorophosphate (DFP), dimethoate, omethoate, chlorfenvinphos, and carbaryl). The fluorescence turn "off-on" response is a consequence of the PET mechanism, supported by the molecular modeling calculations. A limit of detection was calculated to be 1.1 ppm for DFP (a nerve agent simulant). Fluorescence lifetime studies were carried out, which showed significant decay times for **3a**, its oximate, and its DCP-adduct of $\tau = 1.56$, 3.23, and 1.55 ns, respectively, to aid in our understanding of selectivity.

Keywords Organophosphates, nerve agents, molecular sensors, steady-state fluorescence, fluorescence lifetime

1.0 Introduction

The synthesis of Low Molecular Weight Fluorescent probes (LMFPs) to monitor organophosphorus compounds (OPs) is an area of interest [1-4]. The biological effect [5,6] and treatment of organophosphorus poisoning is well known [7,8].

There are several classes of OPs that concern the sensing world; one family of organophosphates is the nerve agents. These include the G-, V- and A-series (Fig. 1), with Novichok molecules purported to be in the latter class. The LD_{50} values of G-series agents are between 5.0 and 24 $mg \cdot kg^{-1}$; the V-series agents are five to ten times lower; for example, VX has an LD_{50} of 0.14 $mg \cdot kg^{-1}$. Another measure of the nerve agents' pernicious nature are the LCt_{50} values, found to be 400 $mg\text{-}min \cdot m^{-3}$ for G-series agents and 10.0 $mg\text{-}min \cdot m^{-3}$ for V-series agents in humans, suggests that these molecules are highly toxic [9]. Novichok agents are significantly more toxic, with reported LD_{50} and LCt_{50} values for Novichok A230 as low as 7.5×10^{-4} to 0.002 $mg \cdot kg^{-1}$ and 1.9 to 3.0 $mg\text{-}min \cdot m^{-3}$, respectively [10]. This is of concern, and of importance to the sensor community, as it has been alleged that Novichok agents have been used in the UK and elsewhere in recent years [11].

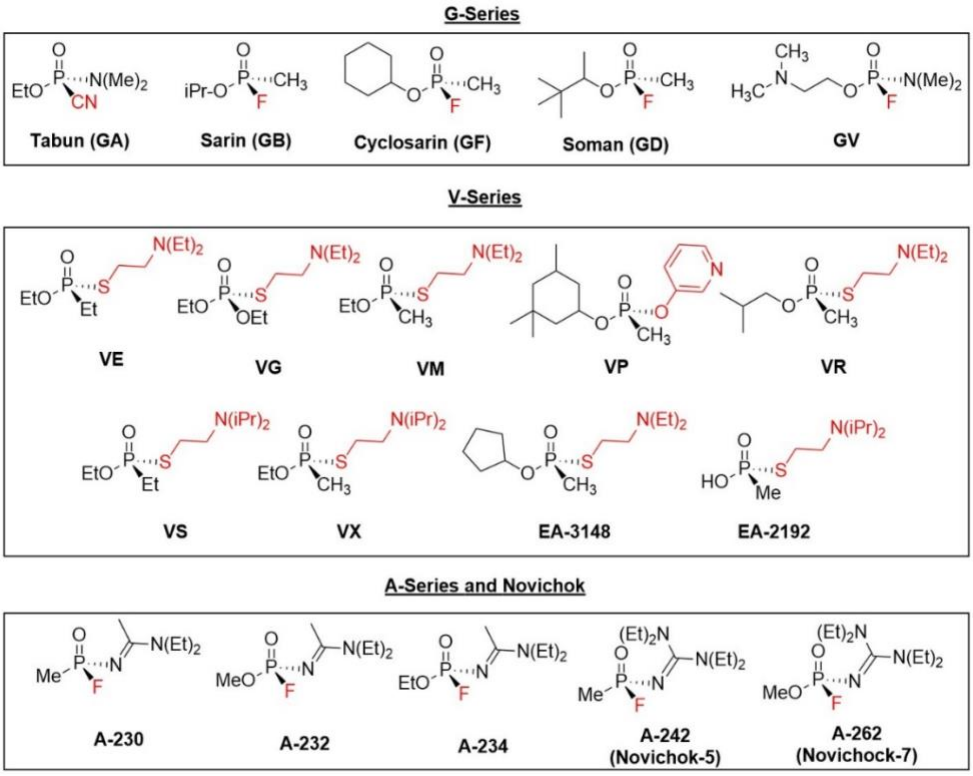

Fig. 1. Three different classes of Nerve Agents.

Over the last several decades, many sensing methods have been developed to monitor and detect OPs. For example, colorimetric detection [12], biosensors [13], immunosensors [14], enzymatic assay [15], electrochemical detection [16,17], electrophoresis techniques [18], and liquid crystal supported thin film surfaces [19] have all been used as techniques to monitor nerve agents. However, these methods have at least one of the following limitations: low selectivity and sensitivity, complexity, they need expert personnel to operate the instruments, slow response time, low limit of detection, and the instruments are not portable.

Many fluorescence probes have been developed [20]. The oxime moiety has been incorporated onto the organic scaffolds of LMFPs which detect Chemical Warfare Agents (CWAs) simulants using colorimetric [12], fluorescent [21,22], and chemiluminescent [17] responses. Another approach that has been utilized in the sensor community is a combination of steady-state fluorescence coupled with lifetime fluorescence techniques. This combination makes it a more powerful detection method. Fluorescence lifetime (τ) measurement is particularly attractive, as the technique is susceptible to the molecular orbital environment. Upon the addition of analytes to a fluorophore, the HOMO-LUMO orbitals energy are affected resulting in the changes in the time that the electrons stay in the excited state and decay back to the ground state. Lifetime experiments have been used to monitor binding events between molecular probes and analytes, for example, pH-dependent sensing [23], ion detection, cell imaging [24], oxygen sensing, and small molecular FRET assay imaging [25].

As part of our ongoing interest in designing and synthesizing LMFPs, we report the synthesis of three coumarin-enamine derivatives. The coumarin moiety has well established photophysical properties. These organic scaffolds have been extensively used in LMFPs to detect metals such as Cu^{2+} and Hg^{2+} [26,27], amino acid recognition [28], and cell imaging [29]. An unusual derivative of the coumarin moiety, the coumarin-enamine, has recently been used to monitor levels of Al^{3+}ions [30] and our group has used a coumarin-enamine derivative to detect the cyanide ion selectively and discriminate structurally similar divalent metals in a sensor array approach [31,32]. Here we report optical studies of a small family of coumarin-enamine molecular probes, and the changes in their UV-vis and fluorescence response (steady-state and lifetime) in a range of solvents, together with the signal change that occurs on the addition of OPs.

2.0 Experimental

2.1 Materials & Methods

All chemicals and solvents were purchased from either Sigma Aldrich, Acros Organic, Honeywell Fluka, Fisher chemical, and Cambridge isotopes and used as received. Solvents were dried with appropriate drying agents when necessary. NMR data (^{1}H, ^{13}C, ^{13}C APT, HSQC, HMBC) were recorded on Bruker AVANCE 600 MHz spectrometer or a Bruker AVANCE 400 MHz spectrometer in the appropriate deuterated solvents. Chemical shifts are reported in parts per million (ppm), where tetramethylsilane (TMS) is the internal standard and coupling constants (*J*) are reported in hertz (Hz). The ^{1}H NMR multiplicities are reported as 'br' (broad), 's' (singlet), 'd' (doublet), 'dd' doublet of doublets, 't' (triplet), 'q' (quartet), and 'm' (multiplet). All spectra are recorded at ambient temperature unless otherwise stated. IR spectra were recorded on a Nicolet Summit FT-IR paired with a Smart Orbit ATR attachment. The characteristic functional groups are reported in wavenumbers (cm^{-1}) and are describes as weak (w), medium (m), strong (s), and very strong (vs). UV-vis experiments were carried out on Evolution 300 UV-vis. Fluorescence experiments were carried out on a PTI QuantaMaster™ 40 intensity-based spectrofluorometer from Horiba in the steady-state. Lifetime fluorescence was carried out using a DeltaFlex™ equipped with a picosecond photon detection module (PRO 850) and Nano-lead head laser source (300 nm) from Horiba. Low-resolution mass spectra (LRMS) were recorded using positive mode electrospray ionization (ESI) on a Thermo Finnigan LXQ. High-resolution mass spectra (HRMS) analysis was completed using positive-ion mode or negative-ion mode electrospray ionization (ESI) with an Apollo II ion source on a Bruker 10 Tesla APEX -Qe FTICR-MS, recorded at Old Dominion University.

2.2 Molecular modeling

Tautomers and isomers of molecular structures (supporting information, Scheme S1) were built in *Spartan '18* [33]. Their geometries were optimized by molecular mechanics (MMFF) and then subjected to conformational analysis. The lowest energy conformer for each structure was determined and used as the input for the higher-level calculations. Two sets of calculations were undertaken, the first in the gas phase (HF/3-21G*) and the second using the conductor-like polarizable continuum model (C-PCM) (HF/3-21) to mimic acetonitrile.

2.3 Synthesis and characterization

Synthesis of 7-*bis*(ethylamino)-4-hydroxycoumarin (1) [31]. 3-Diethylaminophenol (3.30g, 20.0 mmol) was added to a solution of bis-(2,4,6-trichlorophenyl)malonate, known as magic malonate (synthesized based on prior literature [21]) (9.26 g, 20.0 mmol) and anhydrous toluene (50 mL). The reaction mixture then was refluxed for three hours with constant stirring. After this time, the reaction mixture was allowed to cool to room temperature. The precipitate was collected by vacuum filtration and washed with cold toluene. Yield (3.41g, 73%). ^{1}H-NMR (400 MHz, DMSO-d_6, 300 K): δ 7.55 (d, J = 9.0 Hz, 1H), 6.66 (d, J = 9.0 Hz, 1H), 6.45 (s, 1H), 5.23 (s, 1H), 3.39 (q, J = 7.0 Hz, 4H), 1.11 (t, J = 6.8 Hz, 6H); ^{13}C NMR (100 MHz, DMSO-d_6, 300 K): 166.9, 163.3, 156.6, 151.3, 124.6, 108.6, 103.9, 96.9, 86.6, 44.4, 12.8.

General synthesis of compounds 2a-c [21]**.** A solution of 4-aminoacetophenone (1.35 g, 10.0 mmol) in ethanol (10 mL) was added to a solution of desired amine hydrochloride salt (hydroxylamine, methoxylamine, or hydrazine) (20.0 mmol, 2.0 eq) and sodium hydroxide (21.0 mmol)* in water (5 mL) with stirring at room temperature for 18 h. The pH of the solution was adjusted to pH 6 by adding glacial acetic acid, and the volume was reduced under reduced pressure. The concentrated solution was poured into an ice bath. The precipitate was collected by vacuum filtration and recrystallized from a mixture of ethanol-water to produce the desired compounds between 70 and 85% yields.

***** for the preparation of compound **2c**, the concentration of NaOH was doubled due to the use of the dihydrochloride

Characterization of 2a: Yield 1.16 g, 7.72 mmol, 77%; ^{1}H-NMR (400 MHz, DMSO-d_6, 300 K): δ 10.62 (s, 1H), 7.33 (dd, J = 6.6, 2.0 Hz, 2H), 6.53 (dd, J = 6.5, 2.0 Hz, 2H), 5.30 (s, 2H), 2.05 (s, 3H); ^{13}C NMR (100 MHz, DMSO-d_6, 300 K): 153.3, 149.8, 126.9, 124.8, 113.8, 11.8; IR (ATR solid): 3345 (m) & 3289 (m) $\nu_{NH2,}$ 3162 (br) $\nu_{OH(oxime)}$, 1630 (m) $\nu_{C=C}$, 1605 (s) $\nu_{C=N\ (oxime)}$, 1577 (m) $\delta_{NH\ (scissoring)}$ cm^{-1};ESI-LRMS (positive mode): m/z for $[M+H]^+$ = 150.00; ESI-HRMS (positive mode) observed for $[C_8H_{10}N_2O+Na]^+$ = 173.068621; Calculated for $[C_8H_{10}N_2O+Na]^+$ = 173.068534; Elemental analysis (%) calculated for $C_8H_{10}N_2O$: C, 63.98; H, 6.71 N, 18.65; Recalculated for solvent CH_3CH_2OH:H_2O $C_{8.02}H_{10.24}N_2O$: C, 63.26; H, 6.78 N, 18.40; Found for $C_{8.02}H_{10.24}N_2O$: C, 63.09; H, 6.66 N, 18.32.

Characterization of 2b: Yield 1.22 g, 7.43 mmol, 74%; ^{1}H-NMR (400 MHz, DMSO-d_6, 300 K): δ 7.35 (dd, J = 9.1, 2.4 Hz, 2H), 6.54 (dd, J = 9.2, 2.4 Hz, 2H), 5.39 (s, 2H), 3.83 (s, 3H), 2.06 (s, 3H); ^{13}C NMR (100 MHz, DMSO-d_6, 300 K): 154.1, 142.0, 129.6, 127.4, 118.7, 61.9, 12.6. IR (ATR solid): 3411 (w) & 3324 (m) $\nu_{NH2,}$ 2821 (m) ν_{CH}, 1634 (w) $\nu_{C=C}$, 1601 (m) $\nu_{C=N\ (mthyloxime)}$, 1569 (m) $\delta_{NH\ (scissoring)}$ cm^{-1}. ESI-LRMS (positive mode): m/z for $[M+H]^+$ = 165.08; ESI-HRMS (positive mode) observed for $[C_9H_{12}N_2O+Na]^+$ = 187.084219; Calculated for $[C_9H_{12}N_2O+Na]^+$ = 187.084184; Elemental analysis (%) calculated for $C_9H_{112}N_2O$: C, 65.83; H, 7.37; N, 17.06; Recalculated for solvent H_2O $C_9H_{12.4}N_2O$: C, 64.42; H, 7.45 N, 16.69; Found for $C_9H_{11.6}N_2O$: C, 64.60; H, 7.25 N, 16.34.

Characterization of 2c: Yield 1.21 g, 8.12 mmol, 81%; ^{1}H-NMR (400 MHz, DMSO-d_6, 300 K): δ 7.62 (d, J = 8.3 Hz, 2H), 6.58 (d, J = 8.2 Hz, 2H), 5.51 (s, 2H), 2.23 (s, 3H); ^{13}C NMR (100 MHz, DMSO-d_6, 300 K): 158.6, 150.6, 128.1, 126.2, 113.6, 14.5. IR (ATR solid): 3484 (m) & 3422 (m) $\nu_{NH2\ (hydrazone)}$, 3388 (m) & 3343 (m) ν_{NH2}, 1642 (m) $\nu_{C=C}$, 1608 (s) $_{C=N\ (hydrazone)}$, 1586 (s) $\delta_{NH\ (scissoring)}$, 1559 (m) $\delta_{NH\ (scissoring)}$ cm^{-1}; ESI-LRMS (negative mode): m/z for $[(2M-NH_2)-H]^-$ = 264.89; ESI-HRMS (negative mode) observed for a dimer $[2(C_8H_{11}N_3-NH_2)-H]^-$ = 265.145872; Calculated for $[2(C_8H_{11}N_3-NH_2)-H]^-$ = 265.145870

General synthesis of coumarin-enamine derivatives molecular probe 3a-c [31] 7-*bis*(ethylamino)-4-hydroxycoumarine (**1**) (1.0 mmol), and the appropriate primary amine (**2a-c**) (1.0 mmol) and triethyl orthoformate (1.5 mmol) were combined and refluxed in iso-propanol (7.0 mL) for 15 h with constant stirring. After this time, the reaction mixture was allowed to cool to room temperature, and the resulting solid was collected by vacuum filtration and washed with cold iso-propanol. Typical yields 81-89%.

Characterization of 3a: Yield 349 mg, 0.89 mmol, 89% yield; ^{1}H-NMR (600 MHz, DMSO-d_6, 300 K) and ^{13}C NMR (150 MHz, DMSO-d_6, 300 K): See supporting information table S1 and figures S2-S12 for 1D and 2D spectrum. ESI-MS (positive mode): m/z for $[M + H]^+$ = 394.17; IR (ATR solid): 3218 (br) $\nu_{OH(oxime)}$, 2978 (w) ν_{CH}, 1687 (m) ν_{CO} (delta lactone), 1597 (s) ν_{CO} (ketone) cm^{-1}; ESI-HRMS(positive mode) observed for $[C_{22}H_{23}N_3O_4+H]^+$ = 394.175991; Calculated for $[C_{22}H_{23}N_3O_4+H]^+$ = 394.176133.

Characterization of 3b: Yield 332 mg, 0.81 mmol, 81% yield; ^{1}H-NMR (400 MHz, DMSO-d_6, 300 K, assignment of major *E*-(keto) enamine isomer): δ 13.53 (d, *J* = 13.6 Hz, 1H, NH), 8.78 (d, *J* = 13.4 Hz, 1H, $CH_{enamine}$), 7.84-7.69 (m, 2H, $CH_{aromatic}$), 7.67-7.56 (m, 3H, $CH_{aromatic}$ and $CH_{coumarin}$), 7.12 (d, *J* = 7.6 Hz, 1H, $CH_{coumarin}$), 6.68 (d, *J* = 8.1 Hz, 1H, $CH_{coumarin}$), 3.90 (s, 3H), 3.36 (m, 4H), 2.15 (s, 3H), 1.14 (t, *J* = 6.8 Hz, 3H); and ^{13}C NMR (100 MHz, DMSO-d_6, 300 K): 180.1, 162.9, 160.2, 157.1, 154.0, 153.9, 153.7, 153.1, 139.6, 133.8, 127.5, 119.3, 109.0, 98.1, 96.9, 62.1, 44.6, 12.8, 12.6; ESI-MS (positive mode): m/z for $[M + H]^+$ = 408.25; IR (ATR solid): 3083 (w) $\nu_{C=C(enamine)}$, 2937 (w) ν_{CH}, 1701 (s) ν_{CO} (delta lactone), 1596 (s) ν_{CO} (ketone) cm^{-1}; ESI-HRMS (positive mode) observed for $[C_{23}H_{25}N_3O_4+H]^+$ = 408.191613; Calculated for $[C_{23}H_{25}N_3O_4+H]^+$ = 408.191783.

Characterization of 3c: Yield 334 mg, 0.85 mmol, 85% yield; ^{1}H NMR (400 MHz, $CDCl_3$, 300 K, assignment of major *E*-(keto) enamine isomer): δ 13.72 (d, *J* = 13.0 Hz, 1H, NH), 8.84 (d, *J* = 13.0 Hz, 1H, $CH_{enamine}$), 8.04 - 7.83 (m, 3H, $CH_{aromatic}$ and $CH_{coumarin}$), 7.35 (d, *J* = 8.1 Hz, 2H, $CH_{aromatic}$), 6.58 (d, *J* = 8.7 Hz, 1H, $CH_{coumarin}$), 6.37 (s, 1H, $CH_{coumarin}$), 3.44 (q, *J* = 6.7 Hz, 4H), 2.37 (s, 3H), 1.23 (t, *J* = 6.9 Hz, 3H); ^{13}C NMR (100 MHz, $CDCl_3$, 300 K): 181.0, 164.6, 157.4, 155.0, 153.1, 152.9, 151.5, 139.2, 136.5, 128.5, 117.7, 108.8, 108.5, 98.7, 97.2, 44.9, 14.9, 12.5; ESI-MS (positive mode): m/z for $[M + H]^+$ = 393.33; IR (ATR solid): 3352 (w) & 3206 (m) $\nu_{NH2\ (hydrazone)}$, 3066 (w) $\nu_{C=C(enamine)}$, 2975 (w) ν_{CH}, 1715 (s) ν_{CO} (delta lactone), 1581 (s) ν_{CO} (ketone) cm^{-1}; ESI-HRMS (positive mode) observed for $[C_{22}H_{24}N_4O_3+H]^+$ = 393.191916; Calculated for $[C_{22}H_{24}N_4O_3+H]^+$ = 393.192117.

.

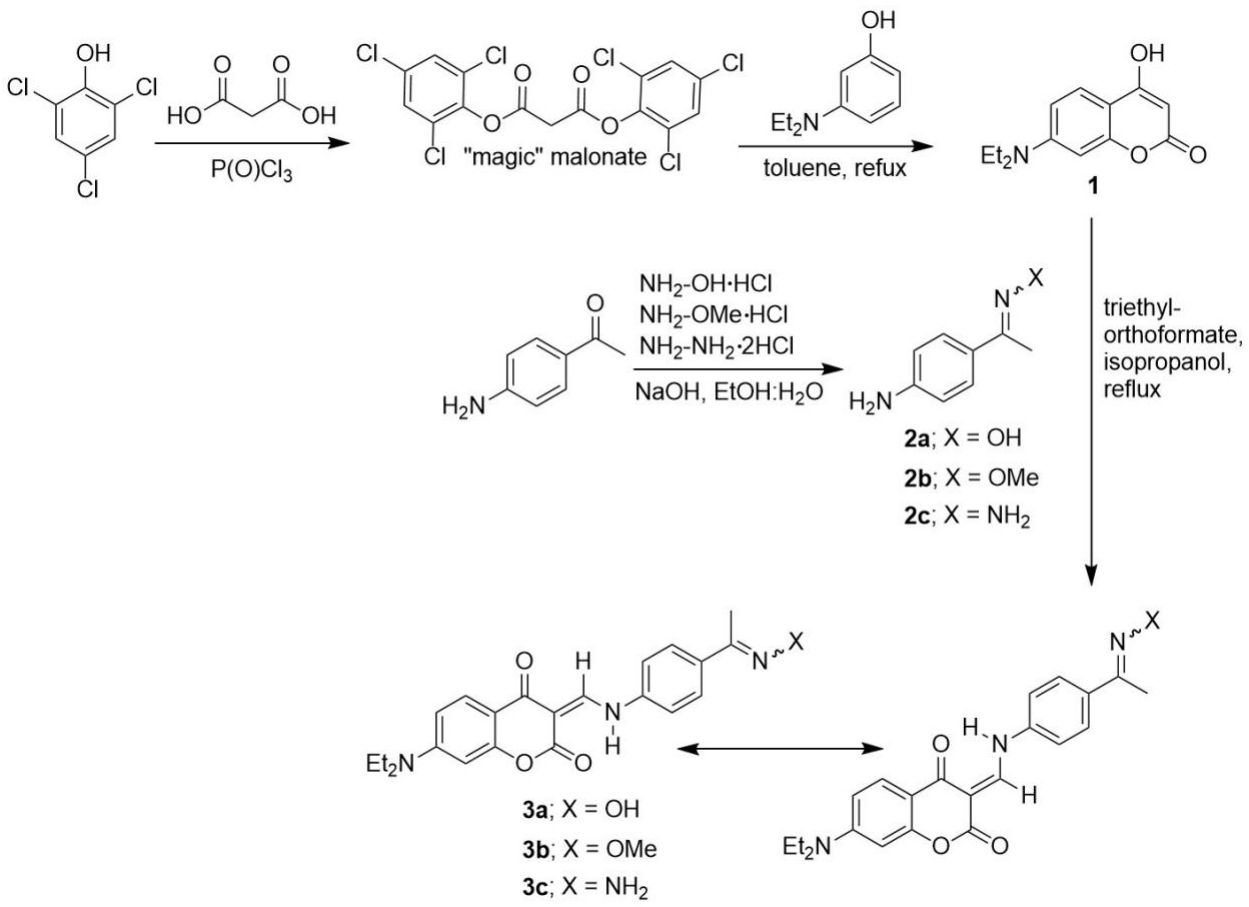

Scheme 1. Synthetic scheme of LMFPs **3a-c**.

3.0 Results & Discussion

*3.1 Synthesis of Low Molecular Weight Fluorescent Probes (**3a-c**)*

Three LMFPs coumarin-enamine compounds were prepared in four steps (Scheme 1). The LMFP **3a** contains the oxime moiety (supernucleophile), which has been incorporated into the organic scaffolds for the monitoring of nerve agents [21,34]. As part of our interest in designing and synthesizing molecular probes, we prepared novel coumarin-enamine oxime **3a**. Another supernucleophile moiety (hydrozone) was also incorporated into the organic scaffolds to give **3c**. Solution studies in DMSO also revealed that compounds **3a-c** each existed in two isomers. It was anticipated that tautomeric transformation can occur; however, the *E*-(keto) enamine-anti-ketoxime and *Z*-(keto) enamine-anti-ketoxime were the only species observed in the NMR (^{1}H NMR, ^{13}C NMR, ^{13}C APT, HSQC, HMBC) studies [31]. Ratio of the *E*-(keto) enamine-anti-

ketoxime and *Z*-(keto) enamine-anti-ketoxime isomers were found to be 3:1 by the integration of ^{1}H NMR of **3a** in DMSO-d_6, which is supported by other coumarin-enamines [31,35].

*3.2 Photophysical Properties of LMFPs **3a-c***

A full solvent study is frequently omitted in the sensing community. Often, only a single solvent system or an aqueous-organic mix is reported so, before investigating the optical response with organophosphates, we carried out an initial photophysical study of **3a** in different solvent systems. The photophysical studies have been carried out on a plethora of coumarin derivatives and are well studied [36]. It is known that the polarity of the solvents significantly influences the photophysical properties of coumarin chromophores, such as their Stokes' shifts and fluorescence lifetimes [37,38]. There are, however, limited solvent studies on the coumarin-enamine moiety containing molecules [31]. The dipole moment of these compounds will influence by solvents; hence the Stokes' shift. Compound **3a** has several functional groups that will change its dipole moment. The dipole moment is significantly changed due to the *keto-enol* tautomerization of the molecular probe **3a.** Moreover, the Stokes' shift increases as the solvent polarity increases (supporting information table S2 and table S3, and Figs. S13(A)-(J), S14 and S15).

In our previously reported coumarin-enamine system, a negative solvatochromic, i.e., a hypsochromic shift, is observed in the absorbance spectrum but, interestingly, this negative solvatochromisim was not seen in this current work [31]. This is unsurprising as the ring system of the coumarin-enamine framework is subtly different, i.e., there is no heteroatom (a nitrogen atom) in the ring system (supporting information Fig. S17-for structures). Consequently, the HOMO of **3a** is significantly stabilized by solvent molecules than the LUMO energy level. Furthermore, the emission spectrum exhibits significant solvent effects whereby a bathochromic shift occurs as the polarity of the solvents increase, (see supporting information Table S2 and Fig. S14) This phenomenon is consistent with other coumarin derivatives containing a dialkylamino substituent at position-7 on the coumarin scaffold. This is a consequence of the dialkylamino group's electron-donating nature that can exhibit a non-planer or planer structure of the coumarin [39]. Whereby, the dialkylamino functional group can be twisted to make the system non-planar; this twisting will form a twisted intramolecular charge transfer (TICT) phenomenon. Whereas the intramolecular charge transfer (ICT) mechanism is stabilized by the solvent, which leads to the stabilization of the LUMO energy level in the case of the planar dialkyl amino group [37,38].

The effect of fluorescence lifetimes (τ) on the solvatochromic outcome was also investigated [37,40,41]. This is the first time that fluorescence lifetimes have been studied in different solvent systems for the coumarin-enamine scaffold to the best of our knowledge. The decay profile for **3a** was fitted to a single exponential function in the different solvent systems. The fluorescence lifetime measurements were carried out and compared to the polarity effect of **3a**. Lifetime decay subtly increases as the solvent polarity increases (see supporting information Fig. S15(B)). Nonpolar solvent has little interaction with the LMFPs, so the lifetime is short (Table S2) yet polar solvents affect the excited state by forming longer-lived excited-state species, which means the electrons in the excited state take longer to reach the ground state. Interestingly the longest lifetime was seen for acetone (τ = 3.778 ns), suggesting that this solvent might be stabilizing the different conformers in solution, forming a number of excited-state species producing many nonradioactive processes [37].

*3.2.1 Calculating Fluorescence Quantum Yields for Probes **3a**, **3b**, and **3c***

The fluorescence quantum yield (ϕ_F) is arguable one of a fluorescent molecule's most important physical characteristics. The ϕ_F is used in calculations to obtain quenching-rate constant [42], energy transfer, rate constants (radiative and non-radiative) [43], and lasing properties [44]. The relative quantum yield is more typically reported in literature. Moreover, many reported fluorescent quantum yields only use one reference or the incorrect reported value in the literature [45].

The ratio of photons absorbed to photons emitted by fluorescence is known as the fluorescence quantum yield (ϕ_F). The value obtained gives the probability of the excited state being deactivated by fluorescence and not by another, non-radio-active mechanism. Williams et al. established the most reliable method to calculate the ϕ_F. Two well-known standards are used with known ϕ_F values; this comparative method yields the most precise calculated values [46].

Two standard samples were chosen to calculate ϕ_F; these reference compounds should be molecules that absorb at the excitation wavelength similar to the chosen unknown sample. The standards should be well characterized and agree with the literature. The two standards chosen for this study are quinine sulfate in 0.1 M H_2SO_4 (ϕ_F = 0.54) [45] and anthracene in ethanol (ϕ_F = 0.27)

[45]. Even though the quantum yield is an excellent photophysical property, care must be taken when performing these experiments as the quantum yield can be easily distorted, and the calculated value might have errors greater than 10 %. The error can arise due to many factors, such as the absorbed intensity, inner filter effects (pre-and post-filter), poor dissolution, oxygen (a non-quencher) in the sample, any impurities, polarization effects, and Raman scattering and photochemical stability. To reduce reabsorption effects, the excitation wavelength's absorption should not exceed 0.1 absorbance units in a 10 mm cuvette [47]. Greater than 0.1 absorbance units result in non-linear effects that may be seen due to inner filter effects, thus perturbing the calculated quantum yields.

The quantum yields obtained for **3a** (DMSO), **3b** (CH_3CN) and **3c** ($CHCl_3$) are 0.83, 0.56, and 0.35, respectively, Table 1 and see supporting information Fig. S16. As the reference compound error falls in the range of 5 to 7 %, below the acceptable 10% error, there is a high degree of confidence that the calculated values obtained are precise. The difference in ϕ_F is due to the supernucleophile moiety on the molecular probe, as the organic framework is the same in all three molecular probes. The molecular probe's planarity is stabilized by a robust intramolecular hydrogen bonding interaction, forming a pseudo ring system. The ketoxime on LMFP **3a** has the highest ϕ_F yield (0.83) which is significantly higher than other published coumarin and coumarin-enamine molecules [48]. The ϕ_F yield for **3b** is lower than **3a**; the ketoxime functional group does not PET quench the fluorescence of the fluorophore. However, the methyloxime group is moderately electron-donating, pushing the electron density towards the nitrogen atom on the methyloxime group. The build-up of the electron density on nitrogen atom can PET quench the fluorescence signal; thus, the lower quantum yield obtained. The hydrazone group in molecular probe **3c** has a drastically lower ϕ_F yield (0.35) due to the amine group's PET quenching ability, a well-known functional group to PET fluorophores [49,50]. The higher the ϕ_F yield, the more desirable the compound is in molecular sensor design, as the molecule will emit stronger fluorescence, helping to monitor analytes at low concentrations to improve LoD. Therefore, only LMFP **3a** and the model system were used for the following studies.

Table 1: Quantum yield data obtained for compounds **3a, 3b,** and **3c.**

Compound	Anthracene	Quinine sulfate	Compound **3a**	Compound **3b**	Compound **3c**
Solvent	EtOH	0.1 M H_2SO_4	DMSO	CH_3CN	$CHCl_3$
Refractive Index of Solvent	1.36	1.35	1.48	1.34	1.45
η^2	1.85	1.82	2.19	1.81	2.09
Literature Q-Yield[45]	0.27	0.54	N/A	N/A	N/A
Gradient	599.4	1293.5	1592.1	1296.3	698.9
Calculated Q-yield					
Anthracene (x)	0.25		0.85	0.57	0.36
Quinine sulfate (x)		0.57	0.80	0.54	0.34
Average			**0.83**	**0.56**	**0.35**

3.2.2 Addition of Organophosphates and Nerve agents

UV-Vis studies: The photophysical studies of **3a** in the various solvent systems described in section 3.2 has given us an insight into the most appropriate solvent system to be used upon the addition of the organophosphate molecules. Dimethylsulfoxide was the solvent choice in these studies as it gives the largest Stokes' shift and is an excellent solvent to aid solubility. To verify whether the LMFP **3a** can act as a colorimetric and a fluorescent sensor for OPs, compound **3a** must be deprotonated to form the supernucleophile required to phosphorolate them. Strong bases such as NaOH are known to undergo phosphorylation reaction with OPs and phosphorous containing nerve agents, such as DFP, and form a less toxic hydrolyzed product, which is the common procedure for decontamination of CWAs [51]. Therefore, a non-nucleophilic strong base was chosen to avoid any acid-base competition between the molecular probe **3a** as both diisopropyl chlorophosphate and DFP are known to have small amounts of HCl and HF, respectively, in solution, even freshly purchased compounds. The non-nucleophilic nitrogen-phosphorous based superbase phosphazene P_4-*t*-Bu solution ($^{DMSO}pK_{BH+}$ = 30.25) was used in these studies [21]. An 8.0 μmol·dm^{-3} solution of **3a** in DMSO was prepared, producing a yellow solution, to which aliquots of P_4-*t*-Bu were added. The initial UV-vis spectrum of compound **3a** shows a broad featureless band at λ_{max} = 410 nm, in DMSO. On the addition of the P_4-*t*-Bu base, the band at 410 nm is hypsochromically shifted, and a band at 372 nm is observed through a distinctive isobestic point at 391 nm (Fig. 2(A)) due to formation of **3a**-oximate, upon the addition of 10 equivalents of HCl to **3a**-oximate of the UV-Vis spectrum, reverted to **3a** (supporting information Fig. S18).

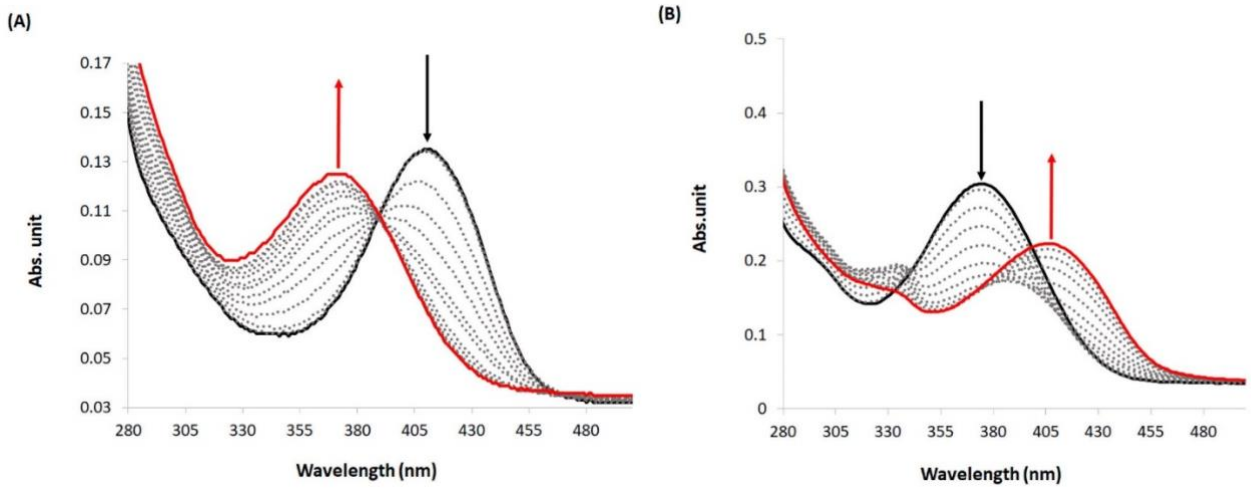

Fig. 2. (A) UV-vis titration of **3a** (8.0 μmol·dm^{-3}) and the addition of 10 equivalents of P_4-*t*-Bu base and (B) the spectroscopic change observed on the addition of DFP (80 μmol.dm^{-3} per aliquot) to **3a**-oximate.

On the addition of aliquots of fresh DFP to a 8.0 μmol·dm^{-3} solution of **3a**-oximate, the band at λ_{max} = 372 nm hypochromoically shifts with a band appearing at 408 nm assigned to the **3a**-DFP adduct, confirmed by ESI-MS (negative mode), whereby an m/z signal is seen at 556 a.u. [**3a**-(DFP-F)-H]$^-$ (supporting information, Fig. S19). The UV-vis titration spectra of **3a** and the other OPs (diisopropyl chlorophosphate, omethoate, dimethoate, chlorfenvinphos, carbaryl, (-)-nicotine, isodrine were investigated (supporting information, Fig. S20). The largest UV-vis spectral changes are seen in the OPs that have a P(V) center with the (-)nicotine showing the smallest change. To investigate which of the OPs gave the most significant colorimetric response, a plot of λ_{max} absorbance difference between the **3a**-oximate (λ_{max} = 376 nm) and the adduct (λ_{max} = 406 nm) is shown in Fig. 3 to give a direct comparison between OPs. The diisopropyl chlorophosphate -adduct exhibited the greatest response ratio, 24.3 times greater than the model (-)-nicotine. DFP is only 7.1 times more responsive, which is reasonable as the diisopropyl chlorophosphate has a better leaving group (Cl^-) than the other OPs.

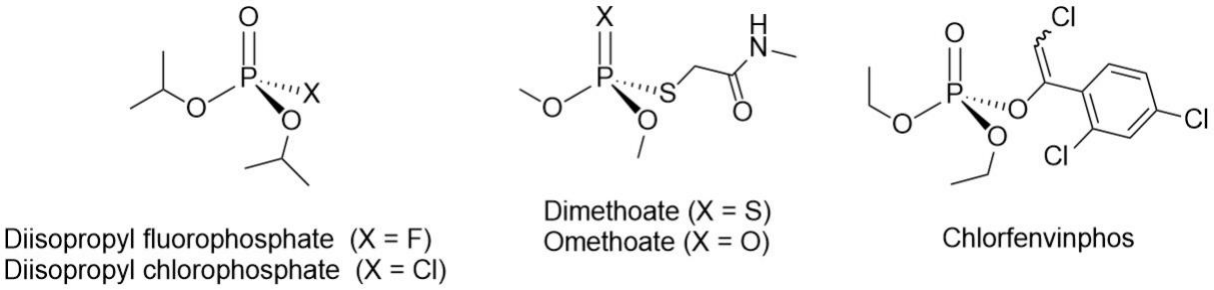

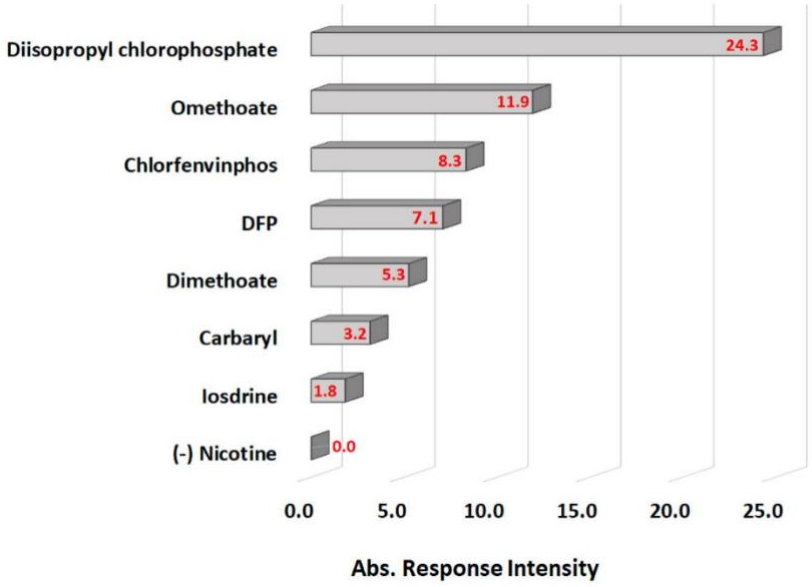

Fig 3. Graph of response ratio between **3a**-oximate ((λ_{max} = 376 nm) plus OPs reactive species (λ_{max} = 406 nm) in DMSO.

Steady-State and Life-time Fluorescence Studies: UV-vis spectroscopy is not as sensitive as fluorescence spectroscopy; therefore, the same spectroscopic studies were carried out by steady-state fluorescence. The addition of P_4-*t*-Bu base is crucial for enamine-based systems as enamine -NH forms an intramolecular six-membered ring with coumarin backbone. Excess P_4-*t*-Bu base can deprotonate the NH proton involved in the RAHB interaction, thus disturbing the conjugation. We have found 10 equivalents of P_4-*t*-Bu base to be optimal, enough to deprotonate the oxime moiety but modestly in excess to 'mop up' excess acid found in the OP samples.

Upon the addition of 10 equivalents of P_4-*t*-Bu **3a** becomes non-fluorescent due to the high energy lone pair on the oximate anion that undergoes PET quenching. The broad emission band at

λ_{em} = 536 nm, the signal is decreased (Fig. 4(A)), producing the "off"-state. Upon the gradual addition of small amounts of reactive OPs the oximate anion undergoes an SN2 reaction with the phosphorous(V) center. Consequently, the energies of the molecular orbitals shift, preventing PET quenching, therefore reinstating the fluorescence intensity and turns "on" the signal (Fig. 7(B), upon the addition of DFP) at 535 nm. The other phosphorus-containing OPs also form adducts but the fluorescence intensity is different (supporting information Fig. S21). The most significant fluorescence responses upon phosphorylation with diisopropyl chlorophosphate, omethoate, or DFP showed an increase in intensities of 18.7, 16.2, and 10.2 fold, respectively (Fig. 5). These large increases in fluorescence intensity are due to the ease of the leaving group upon the phosphorylation reaction; the non-phosphorous containing OPs show significantly reduced fluorescence intensity (supporting information Fig. S21.)

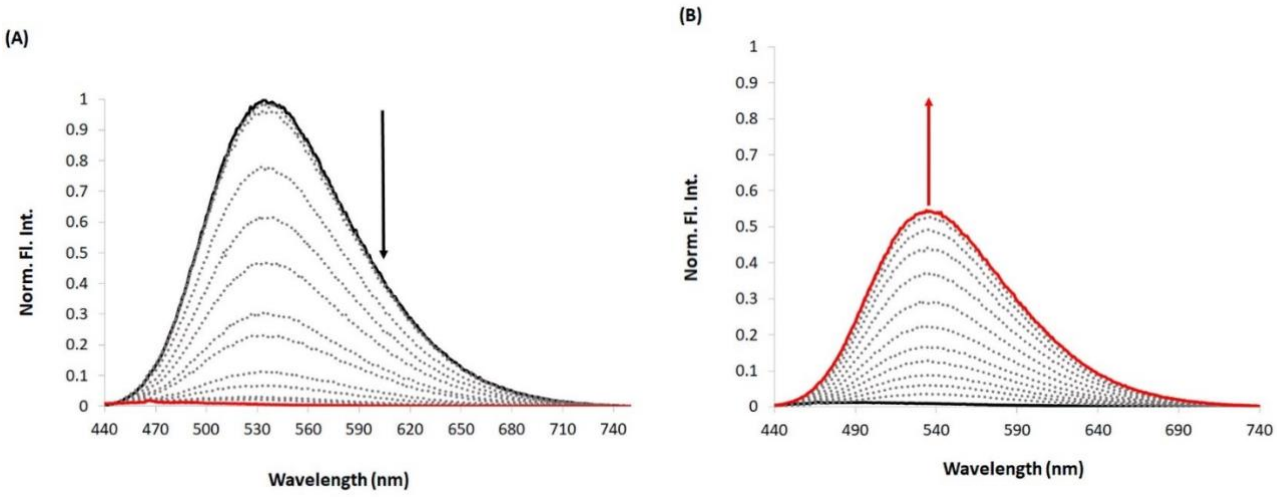

Fig. 4. (A) Ketoximate formation after adding 10 eq. of P_4-*t*-Bu base into **3a** (8.0 μmol·dm^{-3}) (fluorescence turned "off"), (B) reinstating of fluorescence intensity (turned "on") after adding DFP (80 μmol.dm^{-3} per aliquot, λ_{ex} = 410 nm, slovent DMSO).

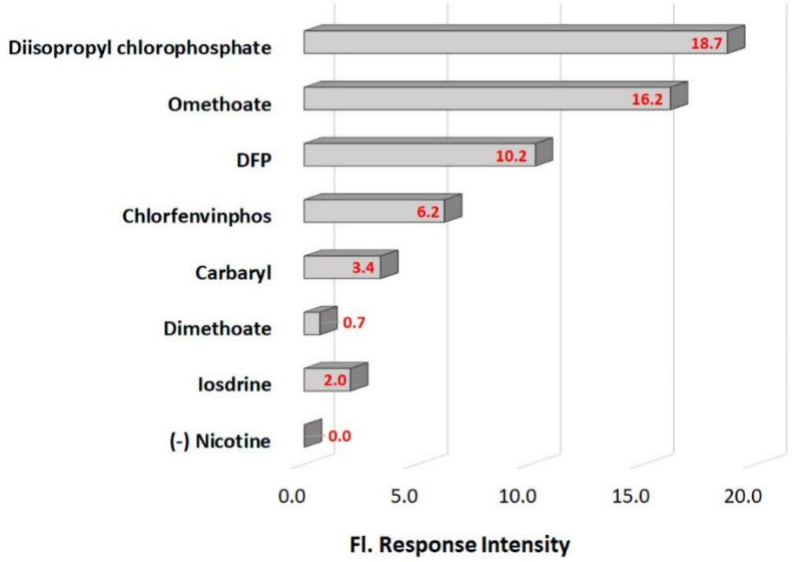

Fig 5. Fluorescence response of **3a**-OPs adduct (Intensity at 535nm, λ_{ex} = 410 nm, solvent DMSO).

Fluorescence lifetimes experiments have become a very useful tool in the molecular sensor community [52-54]. It is a technique that can help selectivity determining the detection of a particular analyte, as the lifetime decay of a specific fluorophore-adduct will be unique under the specific conditions. The fluorescence lifetime experiments were carried out in a DMSO solution (8.0 μmol·dm^{-3}) with the decay profile for **3a** fitted to a single exponential function with a calculated τ = 1.56 ns (supporting information Fig. S22). The decay profile of the mixture (**3a** plus P_4-t-Bu) was fitted to a double exponential (see supporting information Fig. S23) which is typical of mixtures [55]. LMFP **3a** has a high ϕ_F (see Table 1); it is often assumed that the higher the ϕ_F, the longer the lifetime of the fluorophore, but this is not necessarily true, which is demonstrated in this current system. The rigid structure of **3a** lacks any rotational bonds and the planarity of the molecule is helped by the RAHB interaction forming four ring systems (supporting information Fig. S17). Fluorescence lifetimes is the time required for the fluorophore to remain in the excited state, but changes in decay depend on factors, such as temperature, viscosity, and polarity. However, quenchers are arguable one of the most critical factors that will influence the lifetimes. It was anticipated that the PET quenching process in the current system when the oximate is formed would significantly reduce the fluorescence lifetime of the fluorophore, which will be prolonged upon the phosphorylation reaction with the OPs.

The initial lifetime decay (τ_1 = 0.85 ns; Table 2 and supporting information Fig. S23) is a consequence of the **3a**-oximate returning to the ground state. This process is rapid due to the PET quenching mechanism and reduces the lifetime, and this is in agreement with the observed steady-state fluorescence intensity, which is significant due to depopulation (Fig. 6(A)). However, the second decay is significantly larger than the first (τ_1 = 6.36 ns; Table 2) meaning that a fluorescence species is remaining in the excited state for a prolonged period of time. This can be explained by the equilibrium of the conjugate base (**3a**-oximate) and its conjugate acid (P_4-*t*-Bu+H) in solution. The P_4-*t*-Bu is a phosphorous-amine base, and amine functional groups are common quenchers and a responsible for the nonradioactive collisional quenching. Decrease the steady-state fluorescent seen in the emission spectrum, but the aggregation of the fluorophore **3a** and the quencher, allows for excited state to remain populated long enough for a lifetime to be longer. The average decay time is 3.23 ns suggesting that collision quenching has a greater influence on the lifetime decay despite the low emission intensity.

Upon the addition of OPs and nerve agents analogous, except for the carbaryl, lifetimes become shorter due to the depopulation of lone pair in an excited state as ketoximate-adduct formed (Fig. 6(A) and see supporting information Fig.S24-31). The lifetime of the ketoximate-adduct varies slightly as the leaving groups are different for reactive species. For, diisopropyl chlorophosphate (1.56 ns) and DFP (1.55 ns) adduct lifetime is same as **3a** (Table 2), for dimethoate (1.59 ns) and omethoate (1.60 ns), with a sulfur leaving group, it is slightly longer. For chlorfenvinphos (1.92 ns) and carbaryl (6.33 ns), containing aromatic leaving groups, it is longer, as carbaryl can form naphthonal ion. However, (-) nicotine (2.27 ns) does not form adduct as it has no phosphate center, and can't depopulated its excited state, leading to a longer lifetime.

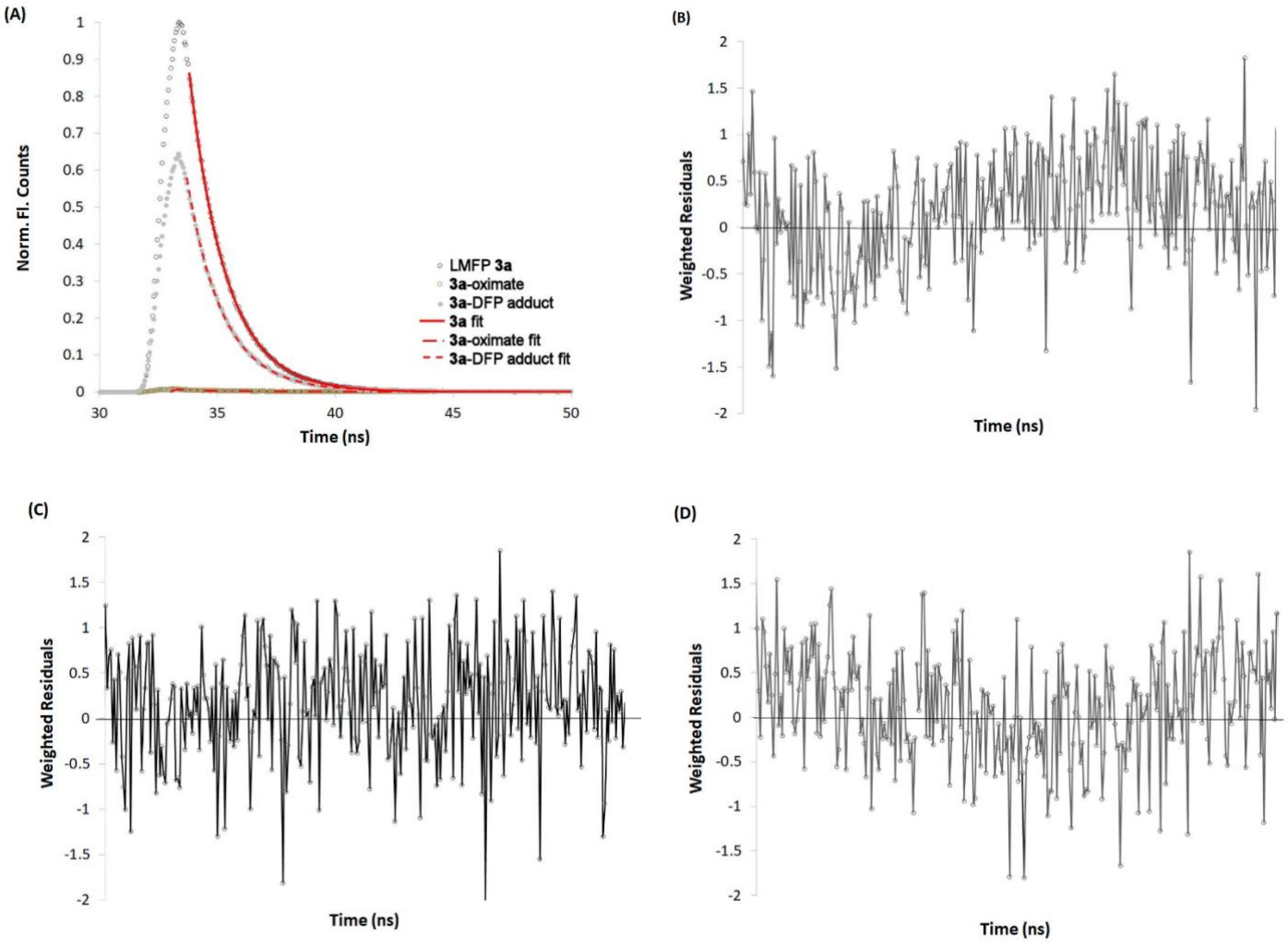

Fig 6. (A) Fluorescence lifetime (τ) of ketoxime (**3a**), ketoximate, and DFP-oximate adduct. (B-D) weighted residuals for **3a**, oximate, and adduct respectively.

Table 2. Fluorescence lifetimes (τ) of various reactive species (average of best two run).

	τ_1(ns) (3σ)	τ_2(ns) (3σ)	$\bar{\tau}$(ns) (3σ)	A (3σ)	χ^2
3a	1.56 (±0.010)	N/A	1.56 (±0.010)	4.80 (±0.575)	1.15
3a-oximate	0.85 (±0.527)	6.36 (±1.560)	3.23 (±1.460)	1.26 (±0.397)	1.18
carbaryl	3.55(±0.298)	18.65(±2.023)	6.33 (±2.045)	1.36 (±0.283)	1.06
(-)nicotine	0.89 (±0.083)	5.37 (±0.162)	2.27 (±0.181)	4.38 (±0.480)	1.22
DFP	1.47 (±0.0232)	3.85 (±0.470)	1.55 (±0.471)	3.34 (±0.400)	1.11
Chlorfenvinphos	1.58 (±0.023)	7.37 (±0.223)	1.92 (±0.224)	2.22 (±0.361)	1.09
Omethoate	1.60 (±0.013)	N/A	1.60 (±0.013)	5.06 (±0.639)	1.10
Dimethoate	1.57 (±0.036)	7.14 (±3.397)	1.59 (±1.708)	3.29 (±0.597)	1.05
Diisopropylchlorophosphate	1.56 (±0.010)	N/A	1.56 (±0.010)	5.47 (±0.676)	1.10
Isodrine	1.02 (±0.176)	2.35 (±0.129)	1.45 (±3.634)	5.03 (±0.507)	1.15

Theoretical Calculations: In their comparative analysis of electrostatic potential maxima and minima, Riley *et al.* [56] found that the results were similar for HF, DFT/B3LYP, or M06-2X methods when the same basis set was used. The STO-3G basis set was unreliable, but the simplest split-valence basis sets, 3-21G and 3-21G*, were found to give excellent results. Surprisingly, larger basis sets showed no improvement for systems involving only first row elements and hydrogen. The same approach has, therefore, been employed here.

To understand the photophysical changes that are observed for LMFP **3a**, quantum mechanical (HF) calculations were carried out (see section 2.2 for details). As compound **3a** can potentially exist in a number of isomers and tautomers, the lowest energy conformer was identified and used for further calculations. The Z/E-(enol) enamine-anti-ketoximes were found to be the most thermodynamically stable. The orbital level diagrams for **3a**, **3a**-oximate and the **3a**-DFP adduct were generated to give the HOMO and LUMO for each species and identify which orbital participates in photoexcitation and photoluminescence ($S_0 \leftarrow S_1$) (Fig. 7 and see supporting information Fig. S32).

The fluorescence intensity significantly decreases upon the deprotonation, and the PET mechanism is attributed to the loss in the fluorescence signal. The $HOMO_{(gs)}$ level of **3a** is -7.46 eV. Whereas the $HOMO_{(gs)}$ of **3a**-ketoximate significantly increase to -2.58 eV. Upon phosphorylation, the $HOMO_{(gs)}$ decrease to lower energy of the **3a**-DFP adduct (-4.00 eV), consistent with the PET mechanism (Fig. 7). This is also in excellent agreement with the fluorescence signal observed that is regenerated, however, the intensity of the fluorescence signal is only half that of the observed intensity of the oxime. Mimicking the solvent system used and the same trend is seen (see supporting information, Table S3).

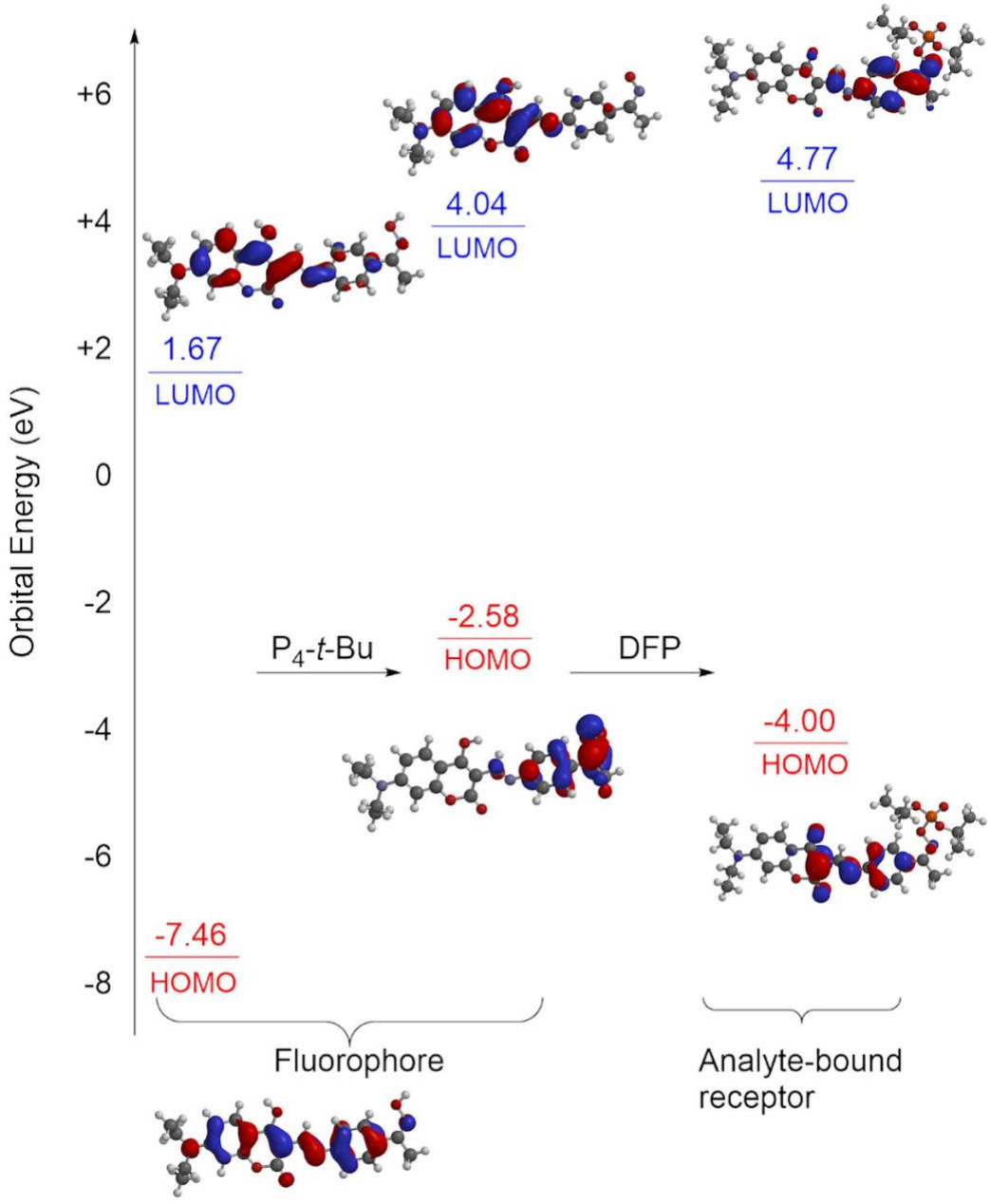

Fig. 7 Molecular orbital energy diagram shows the relative energy of the FMO for **3a**, **3a**-oximate, and **3a**-DFP adduct.

Control experiments were carried out with **3b** (ketomethyloxime), whereby a solution of 8×10^{-6} mol·dm^{-3} in DMSO of **3b**, was prepared. The UV-vis spectrum shows two bands λ = 337 and 403 nm, consistent with the solution's tautomers. The strong, steady-state fluorescence spectrum shows an emission band at λ_{em} = 540 nm, upon the addition of 0.8 mmol·dm^{-3} of the nerve agent

simulant DFP whereas both the UV-vis and emission spectra remained unchanged (supporting information, Fig. S33). Unfortunately, **3c** did not show any optical changes. This confirms that the oximate is needed for the optimal spectroscopic response to be seen upon phosphorylation.

The limit of detection (LoD) was determined using least-squares linear regression of y-axis (normalized fluorescence intensity unit) on the x-axis (concentration of DFP) to calculate the statistic variable $S_{y/x}$ = 0.009. This statistical term was then utilized to calculate the standard deviation for the slope and the intercept. The slope's confidence limit is defined as $b \pm t_{sb}$, where t is the t-value taken from the desired confidence level and n – 2 degrees of freedom; a 95% confidence level (t-value 2.776, df = 6) was adopted for our experiment. Therefore, the LoD is the analyte concentration producing a signal equal to that of the blank signal plus three standard deviations from the blank, which is $y = y_B + 3S_B$ (see supporting information Fig S34). The LoD value of **3a** with DFP was calculated to be 6.4×10^{-6} mol.dm^{-3} or 1.1 ppm, comparable to other molecular probes [22].

4.0 Conclusion

There has been a significant amount of interest over the years on preparing new LMFPs for the detection of OPs, specifically nerve agent simulants. In this current study we have shown that a highly fluorescent coumarin-enamine fluorophore (ϕ_F= 0.83) can be synthesized in four steps. The molecular probe can produce a significant fluorescence "turn on" upon phosphorylation with phosphorous containing OPs. The theoretical calculations support the experimental calculations. The detection limit was calculated to be ≈ 1 ppm.

Corresponding Authors

* E-mail for KJW: karl.wallace@usm.edu

ORCID

Karl J. Wallace ORCID identifier is 0000-0003-4541-7523

Peter. J. Cragg ORCID identifier is 0000-0002-6134-2093

Rashid Mia ORCID identifier is 0000-0003-3209-4403

Acknowledgments and Funding

KJW would like to thank the Department of the Army US Army Engineer Research and Development Center ERDC (Contract W912HZ-19-2-0044). PJC thanks the US Army Research Office for funding computational resources (Contract W911NF-15-1-0624).

Declaration of competing interest

The authors are unaware of any competing interests.

Supplementary information

The Supporting Information (PDF) is available free of charge on XXXX at DOI: XXXX

NMR (1D and 2D), mass spectroscopy, absorption and emission spectra (quantum yield calculation), fluorescence lifetime, molecular modelling, and detection limit calculation and plots

Author statement

On behalf of the authors, KJW can state that each author has contributed to the work reported in this study, including experimental work, theoretical work manuscript preparation, and editing.

References

[1] K. Kim; O. G. Tsay; D. A. Atwood; D. G. Churchill, Destruction and detection of chemical warfare agents, Chem. Rev. 111 (9) (2011) 5345-5403.

[2] Y. J. Jang; K. Kim; O. G. Tsay; D. A. Atwood; D. G. Churchill, Update 1 of: Destruction and detection of chemical warfare agents, Chem. Rev. 115 (24) (2015) PR1-PR76.

[3] Sambrook, M.; Notman, S., Supramolecular chemistry and chemical warfare agents: from fundamentals of recognition to catalysis and sensing, Chem. Soc. Rev. 42 (24) (2013) 9251-9267.

[4] Smith, B. M., Catalytic methods for the destruction of chemical warfare agents under ambient conditions, Chem. Soc. Rev. 37 (3) (2008) 470-478.

[5] A. Friboulet; F. Rieger; D. Goudou; G. Amitai; P. Taylor, Interaction of an organophosphate with a peripheral site on acetylcholinesterase, Biochemistry 29 (4) (1990) 914-920.

[6] T-M. Shih; R. K. Kan; J. H. McDonough, In vivo cholinesterase inhibitory specificity of organophosphorus nerve agents, Chem.-Biol. Interact. 157 (2005) 293-303.

[7] T. Kobrlova; J. Korabecny; O. Soukup, Current approaches to enhancing oxime reactivator delivery into the brain, Toxicol. 423 (2019) 75–83.

[8] D. E. Lorke; H. Kalasz; G. A. Petroianu; K. Tekes, Entry of oximes into the brain: A review, Curr. Med. Chem. 15 (2008) 743-753.

[9] S. Chauhan; R. D'cruz; S. Faruqi; K. K. Singh; S. Varma; M. Singh; V. Karthik, Chemical warfare agents, Environ. Toxicol. Pharmacol. 26 (2) (2008) 113-122.

[10] T. C. C. Franca; D. A. S. Kitagawa; S. F. A. Cavalcante; J.A.V. da Silva; E. Nepovimova; K. Kuca, The Dangerous Fourth Generation of Chemical Weapons, Int. J. Mol. Sci. 20 (2019) 1222-1232.

[11] R. Dixon, R.; L. Morris, Russian opposition leader Navalny poisoned with nerve agent similar to Novichok, Germany says, Washington Post, 2020, https://www.washingtonpost.com/world/europe/navalny-novichok-poisoning-russia/2020/2009/2002/2028ab2099f2010-ed2023-2011ea-bd2008-2021b10132b10458f_story.html.

[12] K. J. Wallace; J. Morey; V. M. Lynch; E. V. Anslyn, Colorimetric detection of chemical warfare simulant, New J. Chem. 29 (2005) 1469-1474.

[13] F. Arduini; A. Amine; D. Moscone; G. Palleschi, Biosensors based on cholinesterase inhibition for insecticides, nerve agents and aflatoxin B1 detection, Microchim. Acta. 170 (2010) 193–214.

[14] G. Liu; J. Wang; R. Barry; C. Petersen; C. Timchalk; P. L. Gassman; Y. Lin, Nanoparticle-based electrochemical immunosensor for the detection of phosphorylated acetylcholinesterase: An exposure biomarker of organophosphate pesticides and nerve agents, Chem. Eur. J. 14 (2008) 9951–9959.

[15] J. Wang; G. Chen; A. J. Muck; M. P. Chatrathi; A. Mulchandani; W. Chen, Microchip enzymatic assay of organophosphate nerve agents, Anal. Chim. Acta 505 (2004) 183–187.
[16] G. Liu; Y. Lin, Electrochemical sensor for organophosphate pesticides and nerve agents using zirconia nanoparticles as selective sorbents, Anal. Chem. 77 (2005) 5894-5901
[17] H. S. Hewage; K. J. Wallace; E. V. Anslyn, Novel chemiluminescent detection of chemical warfare simulant, Chem. Commun. (2007) 3909–3911
[18] J. Wang; M. P. Chatrathi, Capillary electrophoresis microchips for separation and detection of organophosphate nerve agents, Anal. Chem. 73 (2001) 1804-1808.
[19] K. D. Cadwell; N. A. Lockwood; B. A. Nellies; M. E. Alf; C. R. Willis; N. L. Abbott, Detection of Organophosphorous nerve agents liquid crystals supported on chemically functionalized surfaces, Sens. and Actuators B 128 (2007) 91-98.
[20] D. Ajami; J. Rebek Jr, Chemical approaches for detection and destruction of nerve agents, Org. Biomol. Chem. 11 (2013) 3936-3942.
[21] K. J. Wallace; R. I. Fagbemi; F. J. Folmer-Andersen; J. Morey; V. M. Lynch; E. V. Anslyn, Detection of chemical warfare simulants by phosphorylation of a coumarin oximate, Chem. Commun. (2006) 3886–3888.
[22] W. Walton; D. Marauo, D.; L. Munro; V. J. Catalano; P. J. Cragg; M. T. Huggins; K. J. Wallace, A fluorescent dipyrrinone oxime for the detection of pesticides and other organophosphates, Org. Lett. 14 (11) (2012) 2686-2689.
[23] M. Y. Berezin; J. Kao; S. Achilefu, pH-dependent optical properties of synthetic fluorescent imidazoles, Chem. Eur. J. 15 (2009) 3560–3566.
[24] W. Y. Liu; H. Y. Li; B. X. Zhao; J. Y. Miao, Synthesis, crystal structure and living cell imaging of a Cu^{2+}-specific molecular probe, Org. Biomol. Chem. 9 (2011) 4802-4805.
[25] M. Y. Berezin; S. Achilefu, Fluorescence lifetime measurements and biological imaging, Chem. Rev. 110 (2010) 2641–2684.
[26] N. K. Hien; M. V. Bay; N. C. Bao; Q. V. Vo; N. D. Cuong; T. V. Thien; N. T. A. Nhung; D. U. Van; P. C. Nam; D. T. Quang, Coumarin-based dual chemosensor for colorimetric and fluorescent detection of Cu^{2+} in water media, ACS Omega 5 (33) (2020) 21241-21249.
[27] J. M. V. Ngororabanga; Z. R. Tshentu; N. Mama, A new highly selective colorimetric and fluorometric coumarin-based chemosensor for Hg^{2+}, J. Fluoresc. 30 (5) (2020) 985-997.
[28] X. Wu; Q. Wang; D. Dickie; L. Pu, Mechanistic study on a BINOL–coumarin-based probe for enantioselective fluorescent recognition of amino acids, J. Org. Chem. 85 (10) (2020) 6352-6358.
[29] S. Ma; X. Sun; Q. Yu; R. Liu; Z. Lu; L. He, Dihydropyridine-coumarin-based fluorescent probe for imaging nitric oxide in living cells, Photochem. Photobiol. Sci. 19 (9) (2020) 1230-1235.

[30] G. J. Park; H. Y. Jo; K. Y. Ryu; C. Kim, A new coumarin-based chromogenic chemosensor for the detection of dual analytes Al^{3+} and F^{-}, RSC Adv. 4 (109) (2014) 63882-63890.
[31] A. B. Davis; R. E. Lambert; F. R. Fronczek; P. J. Cragg; K. J. Wallace, An activated coumarin-enamine Michael acceptor for CN^{-}, New J. Chem. 38 (10) (2014) 4678-4683.
[32] A. M. Mallet; A. B. Davis; D. R. Davis; J. Panella; K. J. Wallace; M. Bonizzoni, A cross reactive sensor array to probe divalent metal ions, Chem. Commun. 51 (2015) 16948-16951.
[33] Spartan '18 Irvine CA, USA, 2018.
[34] F. Worek; H. Thiermann; T. Wille, Organophosphorus compounds and oximes: a critical review, Arch. Toxicol. 94 (2020) 2275-2292.
[35] V. F. Traven; I. V. Ivanov; V. S. Lebedev; T. A. Chibisova; B. G. Milevskii; N. P. Solov'eva; V. I. Polshakov; G. G. Alexandrov; O. N. Kazheva; O. A. Dyachenko, E/Z (C= C)-Isomerization of enamines of 3-formyl-4-hydroxycoumarin induced by organic solvents, Russ. Chem. Bull. 59 (8) (2010) 1605-1611.
[36] D. Cao; Z. Liu; P. Verwilst; S. Koo; P. Jangjili; J. S. Kim; W. Lin, Coumarin-based small-molecule fluorescent chemosensors, Chem. Rev. 119 (18) (2019) 10403-10519.
[37] S. Nad; M. Kumbhakar; H. Pal, Photophysical properties of coumarin-152 and coumarin-481 dyes: unusual behavior in nonpolar and in higher polarity solvents, J. Phys. Chem. A 107 (24) (2003) 4808-4816.
[38] L. Cisse; A. Djande; M. Capo-Chichi; F. Delatre; A. Saba; A. Tine; J. J. Aaron, Revisiting the photophysical properties and excited singlet-state dipolemoments of several coumarin derivatives, Spectr. Acta. Part A 79 (2011) 428–436.
[39] M. Cigan; J. Donovalová; V. Szöcs; J. Gaspar; K. Jakusová; A. Gaplovsky, 7-(Dimethylamino) coumarin-3-carbaldehyde and its phenylsemicarbazone: TICT excited state modulation, fluorescent H-aggregates, and preferential solvation, J. Phys. Chem. A 117 (23) (2013) 4870-4883.
[40] M. Y. Berezin; H. Lee; W. Akers; S. Achilefu, Near infrared dyes as lifetime solvatochromic probes for micropolarity measurements of biological systems, Biophys. J. 93 (8) (2007) 2892-2899.
[41] J. A. Bautista; R. E. Connors; B. B. Raju; R. G. Hiller; F. P. Sharples; D. Gosztola; M. R. Wasielewski; H. A. Frank, Excited state properties of peridinin: observation of a solvent dependence of the lowest excited singlet state lifetime and spectral behavior unique among carotenoids, J. Phys. Chem. B 103 (41) (1999) 8751-8758.
[42] M. Sadrai; L. Hadel; R. R. Sauers; S. Husain; K. Krogh-Jespersen; J. D. Westbrook; G. R. Bird, Lasing action in a family of perylene derivatives: singlet absorption and emission spectra, triplet absorption and oxygen quenching constants, and molecular mechanics and semiempirical molecular orbital calculations, J. Phys. Chem. 96 (20) (1992) 7988-7996.

[43] Bañuelos, P. J.; F. López Arbeloa; V. Martínez Martínez; L. T. Arbeloa López; I. López Arbeloa, Photophysical properties of the pyrromethene 597 dye: solvent effect, J. Phys. Chem. A 108 (26) (2004) 5503-5508.

[44] T. L. Arbeloa; F. L. Arbeloa; I. L. Arbeloa; I. Garcıa-Moreno; A. Costela; R. Sastre; F. Amat-Guerri, Correlations between photophysics and lasing properties of dipyrromethene–BF_2 dyes in solution, Chem. Phys. Lett. 299 (3-4) (1999) 315-321.

[45] A. M.Brouwer, Standards for photoluminescence quantum yield measurements in solution (IUPAC Technical Report), Pure Appl. Chem. 83 (12) (2011) 2213-2228.

[46] A. T. R. Williams; S. A. Winfield; J. N. Miller, Relative fluorescence quantum yields using a computer-controlled luminescence spectrometer, Analyst 108 (1983) 1067-1071.

[47] S. Dhami; A. J. de Mello; G. Rumbles; S. M. Bishop; D. Phillips; A. Beeby, Phthalocyanine fluorescence at high concentration: dimers or reabsorption effect?, Photochem. Photobiol. 61 (4) (1995) 341-346.

[48] Y. Shiraishi; N. Hayashi; M. Nakamura; T. Hirai, Coumarin–imine–quinoxaline linkage designed based on the strecker reaction as a receptor for fluorometric cyanide anion detection in neutral media, Chem. Lett. 45 (11) (2016) 1294-1296.

[49] A. I. Said; N. I. Georgiev; V. B. Bojinov, A fluorescent bichromophoric “off-on-off” pH probe as a molecular logic device (half-subtractor and digital comparator) operating by controlled PET and ICT processes, Dyes Pigm. 162 (2019) 377-384.

[50] S. Bishnoi, S.; M. D. Milton, Tunable phenothiazine hydrazones as colour displaying, ratiometric and reversible pH sensors, Tetrahedron Lett. 56 (47) (2015) 6633-6638.

[51] Y. C. Yang; J. A. Baker; J. R. Ward, Decontamination of chemical warfare agents, Chem. Rev. 92 (8) (1992) 1729-1743.

[52] H. Szmacinski; J. R. Lakowicz, Fluorescence lifetime-based sensing and imaging, Sens. Actuators, B 29 (1-3) (1995) 16-24.

[53] M. Schäferling, The art of fluorescence imaging with chemical sensors, Angew. Chem., Int. Ed. Engl. 51 (15) (2012) 3532-3554.

[54] H. Zhu; J. Fan; J. Du; X. Peng, Fluorescent probes for sensing and imaging within specific cellular organelles, Acc. Chem. Res. 49 (10) (2016) 2115-2126.

[55] J. R. Lakowicz; H. Szmacinski, Fluorescence lifetime-based sensing of pH, Ca^{2+}, K^{+} and glucose, Sens. Actuators, B 11 (1-3) (1993) 133-143.

[56] K. E. Riley; K-A. Tran; P. Lane; J. S. Murray; P. Politzer, Comparative analysis of electrostatic potential maxima and minima on molecular surfaces, as determined by three methods and a variety of basis sets, J. Comput. Sci. 17 (2016) 273-284.